Application of an imaging plate to electron crystallography at atomic resolution

Tetsuya Ogawa*, Sakumi Moriguchi, Seiji Isoda and Takashi Kobayashi
Institute for Chemical Research, Kyoto University, Uji, Kyoto-fu 611, Japan
(Received 21 June 1993; revised 17 September 1993)

An imaging plate was used to quantitatively measure the electron diffraction intensities of graphite and polyethylene (PE) crystals. After the signs of the structure factors were assigned by using a direct phasing procedure, potential maps were made in order to determine atomic positions. Peaks corresponding to the carbon atoms in graphite were seen at (0,0), (1/3,2/3) and (2/3,1/3) in the map of the *c*-axis projection. For PE, hydrogen atoms were resolved in addition to carbon atoms due to the higher scattering powers of hydrogen for electron beam than for X-ray. The setting angle of the molecular chain in the *c*-axis projection of the unit cell was determined to be 46.0°, which is consistent with the results of X-ray experiments. *R*-factors were found to be 0.228 and 0.197 for graphite and PE, respectively. It is shown that the high sensitivity, the wide dynamic range, the good linear response and the digital output data of the imaging plate are useful for structure analysis using electron diffraction.

(Keywords: imaging plate; electron diffraction; potential map)

INTRODUCTION

In high resolution transmission electron microscopy, many experimental techniques have been developed in order to reduce the electron radiation damage of specimens, because of an increasing need to observe radiation-sensitive specimens such as organic crystals and biological specimens. High voltage electron microscopy, the cryoprotection technique[1] and the minimum dose system[2], which is used to irradiate the field of view only during photography, are often used for such purposes. However, highly sensitive recording materials have continued to be developed, e.g. highly sensitive photographic films, image intensifiers, imaging plates (IPs). Among them, the IP was initially developed as a highly sensitive two-dimensional detector in X-ray radiography[3] in place of conventional X-ray films and was soon applied to the field of X-ray crystallography[4,5], owing to its high quality in quantitative analysis of radiation intensity. Recently, on the grounds of its suitability in electron detection, it has also applied to the field of electron microscopy[6].

The fundamental properties of the IP have been reported by Hayakawa *et al.*[7] and Mori *et al.*[8] for 100–400 keV electron beams and Isoda *et al.*[9,10] for 600–1000 keV beams. The IP has more than two orders higher sensitivity at these accelerating voltages than that of conventional electron microscopic films. It exhibits also a wide dynamic range (about four orders) and a very good linear response to the incident electron dosage in this range. These characteristics are superior to those of other highly sensitive recording materials. At present, in spite of these superior properties, the quality of the image obtained is poorer than that of conventional electron microscopic films, due to the lower resolution. However, the superior properties of IPs can still be used in other applications such as quantitative analysis of images or diffractions. In diffraction observation, the wide dynamic range of four orders may cover the range from strong to weak scattering, and the good linear response and the digital data make it easy to collect the intensity data as output signals.

In the structure determination of very small crystallites or thin layers, e.g. polymer single crystals or pseudomorphic epitaxial layers, electron diffraction might be a better technique to analyse the structures rather than X-ray or neutron diffraction. Although it has been commonly thought that electron diffraction is unfavourable in quantitative data collection, Dorset has recently shown that electron diffraction is useful for crystal structure analysis using the so-called direct phasing procedure[11] as employed in X-ray crystallography[12,13]. Accordingly, quantitative data collection with a good recording medium may be expected to realize reliable structure determination using electron diffraction.

In this paper, the applicability of the IP for the quantitative measurement of electron diffraction intensity was studied. This was done by producing electrostatic potential maps using a direct phasing procedure on the measured intensity data of electron diffraction recorded on an IP.

EXPERIMENTAL

We prepared thin, flaky graphite as a specimen with a simple and well known structure and single crystals of polyethylene (PE) as an example of an irradiation-sensitive polymer crystal, which was grown from dilute xylene solution. It is known that dynamic scattering results in intensity deviations from kinematic values, if specimens are thick and/or contain heavy atoms[14]. The

* To whom correspondence should be addressed

0032-3861/94/06/1132–05
© 1994 Butterworth-Heinemann Ltd

specimens used were <10 nm, so that the dynamic scattering contributions did not significantly affect the accuracy of the structure determination, even when perturbed by multiple scattering.

Figure 1 is a schematic diagram of the experimental procedure. Electron diffraction patterns were recorded on an IP using transmission electron microscopes operated at 800 kV for graphite (JEM-ARM1000, Jeol) and 200 kV for PE (JEM-2000FXII, Jeol), respectively. The transmission electron diffraction experiment was carried out taking extreme care that the orientation of the crystals to the electron beam was corrected to minimize the excitation errors. This was extremely important, since misorientation results in asymmetric diffraction. IP DL-URIII was commercially supplied by Fuji Photo Films Co., and had a 140 μm thick layer which could be photo-stimulated and an effective size of 102 mm × 77 mm. An IP controlling system (PIXsysTEM, Jeol), was used for reading the recorded intensities of the diffraction patterns. The read-out signal data was composed of 2048 × 1536 pixels, where each pixel size was 60 μm × 50 μm. After the data were transformed to electron beam intensities using the calibration line as shown in *Figure 2*, integral intensities were measured for each diffraction spot as follows. Two concentric circular regions were prepared for each diffraction spot at the centre. One was an encircled inner region to integrate intensities. The other was a region around the integral region, where the background level around each spot was determined by least squares fit assuming a relation:

$$I_{bi} = \alpha x_i + \beta y_i + \gamma$$

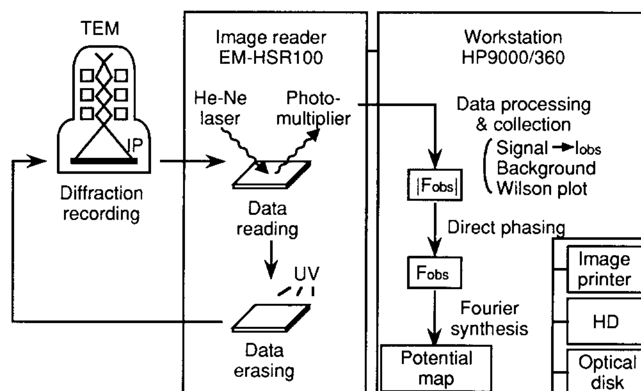

Figure 1 Schematic diagram of the experimental procedure

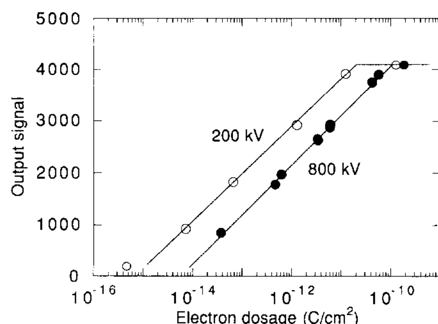

Figure 2 Relationship between electron dosage (Q) and output signal (D) of an IP for two accelerating voltages. The solid lines show the relation: $D = A \log Q + B$, where $A = 966$ and $B = 13\,747$ for 800 kV and $A = 915$ and $B = 13\,851$ for 200 kV

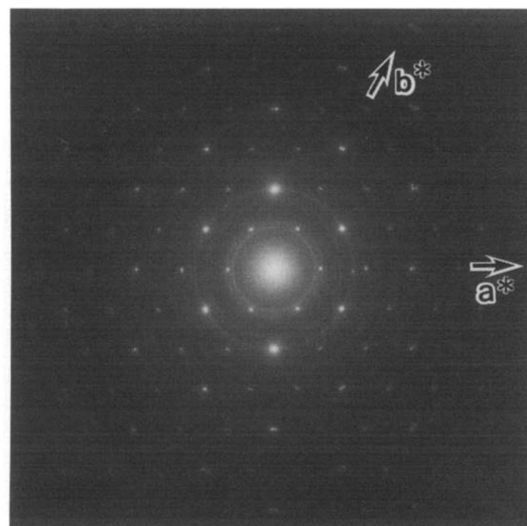

Figure 3 Electron diffraction pattern of graphite with the incident electron beam parallel to the c-axis. The intensities of 130 reflections could be measured with only one sheet of IP due to its wide dynamic range

where I_{bi} is the intensity of the background at the coordinates x_i, y_i of a pixel i in this region on the IP and α, β and γ are constants to be determined. The integral intensities were obtained by summing the pixel data in the encircled integral region and subtracting the background contributions. After the absolute intensities and a mean temperature factor were determined using a Wilson plot, the signs of the structure factors were assigned so that the electrostatic potential map could be synthesized.

RESULTS AND DISCUSSION

The electron diffraction pattern of graphite recorded on an IP is shown in *Figure 3*, where the incident electron beam is parallel to the c-axis. Each $hk0$ diffraction spot splits into several spots owing to the slight disorder of crystal orientations in the specimen. All the integral intensities contained contributions from these small spots. The diffractions from the gold particles used to calibrate the camera length were recorded together in the figure. Although the diffraction from gold is superimposed on that from graphite, the contributions of these diffractions to the integral intensities of graphite were neglected, because their intensities were sufficiently small compared with those of the graphite spots. The integral intensities of 130 diffraction spots were measured over the intensity range of about four orders with only one sheet of IP owing to its wide dynamic range. The spot with the highest scattering vector had a Miller index of 620, which corresponds to a Bragg spacing of 0.0295 nm. A Wilson plot gave a mean temperature factor of 0.0065 nm^2. Finally, 19 symmetrically independent diffraction intensities were obtained. If the same temperature factors are assumed for all atoms, the signs of the structure factors may be assigned plus for all reflections due to the crystal structure of graphite, which is composed of alternate stacking of two honeycomb layers separated by the C–C bond distance. Consequently, the structure factor is obtained as a square root of intensity. *Figure 4a* shows the electrostatic potential map

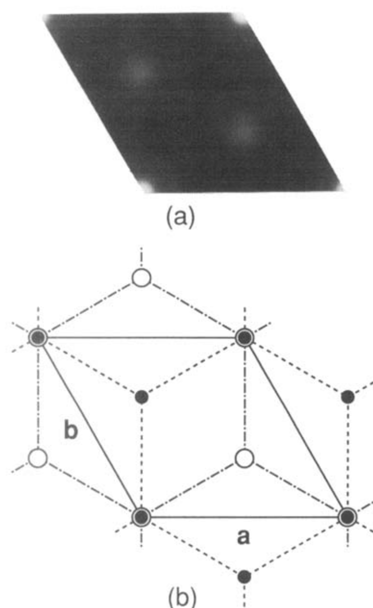

Figure 4 (a) Electrostatic potential map for graphite calculated from observed structure factor magnitudes. The peak at (0,0) is about two times higher than those at (1/3,2/3) and (2/3,1/3). (b) Projection of the graphite crystal structure onto the *ab*-plane; $a=b=0.246$ nm, $c=0.670$ nm

Table 1 Comparison of the observed and calculated structure factors for graphite

h	k	l	$F_{obs.}$	$F_{calc.}$
1	0	0	2.30	3.23
1	1	0	7.91	5.58
2	0	0	1.28	1.21
2	1	0	0.87	0.73
3	0	0	2.01	1.77
2	2	0	1.54	1.27
3	1	0	0.45	0.41
4	0	0	0.37	0.34
3	2	0	0.25	0.28
4	1	0	0.59	0.61
5	0	0	0.18	0.21
3	3	0	0.41	0.42
4	2	0	0.23	0.19
5	1	0	0.11	0.17
6	0	0	0.28	0.26
4	3	0	0.10	0.13
5	2	0	0.17	0.23
6	1	0	0.12	0.11
6	2	0	0.11	0.08

synthesized from the structure factors. Potential peaks corresponding to the carbon atom positions in the unit cell are clearly seen at (0,0), (1/3,2/3) and (2/3,1/3). The peak at (0,0) is about two times higher than those at (1/3,2/3) (2/3,1/3), which means two carbon atoms exist at (0,0) in the unit cell, and one atom is located at (1/3,2/3) (2/3,1/3) as expected from *Figure 4b*. When a least squares fit between the observed and the calculated structure factors was carried out using the scaling factor and different temperature factors for the atomic sites of (0,0) and (1/3,2/3) as fitting parameters, an *R*-factor of 0.228 was obtained for the temperature factors of 0.0030 and 0.0071 nm^2 for the sites (0,0) and (1/3,2/3), respectively. (*Table 1* shows the observed and the calculated structure factors using these values.) This result demonstrates the suitability of an IP for the quantitative detection of the electron beam intensity of diffraction.

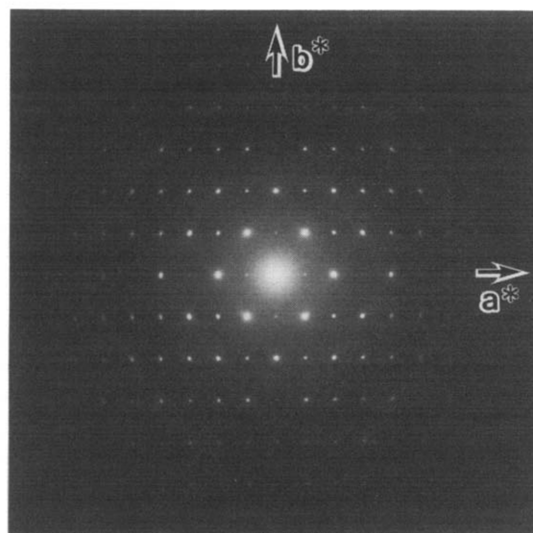

Figure 5 Electron diffraction pattern of a single crystal of PE with the incident electron beam parallel to the *c*-axis. Integral intensities of 164 diffraction spots were obtained from two sheets of IP using exposure times of 0.1 and 4.0 s

Figure 5 shows the electron diffraction pattern of a single crystal of PE. A single PE crystal is a lamellar crystal with a thickness of ~10 nm, with a normal which is almost parallel to the *c*-axis. Hence, *Figure 5* shows the *c*-axis incident diffraction pattern. Owing to the high sensitivity of an IP, in excess of 100 diffraction patterns can be taken in the damage process of PE. In this study, two diffraction images were taken on two separate IPs with different exposure times using an electron current of 1.0×10^{-5} A cm^{-2}. One IP was exposed for 0.1 s to record strong, lower-order reflections and the other was exposed for 4.0 s to record weak, higher-order reflections. Integral intensities of 164 spots (48 symmetrically independent spots) with an intensity magnitude of more than four orders could be measured from these two IP sheets. The Miller index with the highest scattering vector was 650, corresponding to a Bragg spacing of 0.0770 nm. This value is smaller than the expected value of 0.0864 nm for the C–C bond in the projection onto the *ab*-plane. A mean temperature factor of 0.064 nm^2 was obtained by a Wilson plot.

Since the two-dimensional space group of the PE crystal projected onto the *ab*-plane is pgg, the structure factor is a real number. The direct phasing method was used to assign the signs of the observed structure factors[11]. In this space group, the signs of two reflections with indices of $(hk)\neq(gg)$, where g is an even integer, could be assigned arbitrarily in order to define the origin of the unit cell. From these signs, the signs of the other reflections were determined using the $\sum_2$ relationship, $S(h)S(h')S(h+h')=1$ (where $S(h)$ was the sign of reflection h), for the sets of the reflections h, h' and $h+h'$ with large values of the multiples, A, of their normalized structure factors, E:

$$A=\frac{\sigma_3}{\sigma_2^{3/2}}|E(h)E(h')E(h+h')|$$

$$|E(h)|^2=\frac{|F(h)|^2}{\varepsilon\sum f_j(h)^2\exp(-2Bs^2)}$$

$$\sigma_n=\varepsilon\sum_j^N f_j(h)^n$$

Here B is the temperature factor, s is the magnitude of the scattering vector and ε is an integer which is 1 for the reflections with $h \neq 0$ and $k \neq 0$ and 2 for those with $h=0$ or $k=0$ in this space group. $F(h)$ and $f_j(h)$ are the structure factor and atomic scattering factor of the j-atom at the reciprocal vector of h, respectively.

Using these signs and observed structure factors, a potential map is synthesized as in *Figure 6a*. In addition to four clear peaks corresponding to carbon atoms, weak peaks corresponding to hydrogen atoms, which are hardly detected by X-ray, can be seen due to the higher ratio of the scattering amplitude of a hydrogen atom to a carbon atom in an electron beam experiment compared to X-ray. This point is one of the merits of analysing organic crystal structures by electron diffraction. Refinement of atomic positions by a least squares fit was carried out using the different temperature factors for the carbon and hydrogen atoms. The result showed that the setting angle, i.e. the angle between the plane of the zigzag chain and the b-axis was 46.0°. This coincides with the results of X-ray experiments (44–48°)[15–17]. *Table 2* shows the observed and calculated structure factors. The R-factor was 0.197 for temperature factors of 0.063 and 0.093 nm^2 for carbon and hydrogen, respectively. Comparing with X-ray results, there was a little difference in bond length and angle. The C–C bond distance was 0.0815 nm, which was a little shorter than the value of 0.0864 nm from X-ray results. The angle $\angle$HCH was also slightly smaller (105°) than that obtained by X-ray (109.47°). This difference may be due to the lack of corrections made to the intensity data, since corrections were only made for the temperature factors. Even though other corrections, such as dynamic scattering contributions or for the Lorentz factor, may be small, such corrections are necessary in order to obtain accurate values or smaller R-factors, as well as careful selection of observation conditions. For thin crystals, the Lorentz factor is the most important correction to be made. Unfortunately, in the present case, it is difficult to introduce a rigorous Lorentz factor with physical meaning, because of the uncertainty of the shape of the elongated reciprocal lattice points by the bending of the crystal, which has been confirmed by the existence of a slight graduation in the dark field images.

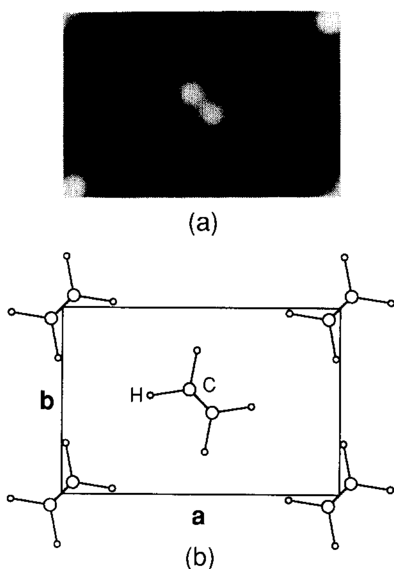

Figure 6 (a) Electrostatic potential map for PE calculated from observed structure factor magnitudes and signs assigned by the direct method. Four peaks corresponding to carbon atoms and weak peaks corresponding to hydrogen atoms can be clearly seen. (b) Projection of the PE crystal structure onto the ab-plane; $a=0.740$ nm, $b=0.493$ nm, $c=0.255$ nm

Table 2 Comparison of the observed and calculated structure factors for polyethylene

h	k	l	$F_{obs.}$	$F_{calc.}$	h	k	l	$F_{obs.}$	$F_{calc.}$
1	1	0	12.41	9.59	5	3	0	0.20	0.21
2	0	0	11.23	8.78	7	1	0	−0.25	−0.11
2	1	0	−1.84	−1.92	4	4	0	0.17	0.07
0	2	0	4.91	4.66	6	3	0	−0.36	−0.38
1	2	0	−1.22	−1.20	1	5	0	−0.30	−0.12
3	1	0	3.21	2.56	7	2	0	−0.22	−0.27
2	2	0	2.58	1.75	2	5	0	−0.17	−0.20
4	0	0	2.18	2.55	5	4	0	−0.31	−0.35
3	2	0	−1.41	−1.33	8	0	0	−0.19	−0.15
4	1	0	−0.94	−1.17	3	5	0	−0.20	−0.09
1	3	0	1.31	1.57	8	1	0	−0.06	−0.12
2	3	0	−0.95	−0.97	7	3	0	−0.12	−0.02
4	2	0	0.87	0.61	6	4	0	0.07	0.02
5	1	0	0.64	0.78	4	5	0	−0.17	−0.18
3	3	0	0.59	0.49	8	2	0	−0.13	−0.09
5	2	0	−0.70	−0.75	0	6	0	−0.16	−0.09
6	0	0	0.32	0.30	5	5	0	−0.09	−0.01
0	4	0	0.32	0.39	1	6	0	−0.04	−0.04
4	3	0	−0.74	−0.71	9	1	0	−0.09	−0.09
1	4	0	−0.31	−0.37	8	3	0	−0.09	−0.10
6	1	0	−0.37	−0.48	7	4	0	−0.12	−0.14
2	4	0	0.33	0.13	2	6	0	−0.11	−0.07
6	2	0	0.26	0.05	9	2	0	−0.04	−0.05
3	4	0	−0.48	−0.51	6	5	0	−0.06	−0.10

CONCLUSIONS

The examples given here are rough estimates of crystal structures with only corrections in the intensities for the temperature factors, so that the R-factors have values of ~ 0.2. Nevertheless, the potential maps show the suitability of the IP in the structure analysis of crystals using electron diffraction. In comparison with conventional electron microscopic films, a large number of diffraction peaks can be recorded on a sheet of IP due to its wide dynamic range and high sensitivity. The digital data have a good linear response to electron dosage and so are easily dealt with by computer. Because of its high sensitivity, the IP is particularly useful in experiments using organic crystals which are easily damaged by electron irradiation. Further structure analysis of organic compounds is currently underway, and some unknown crystal structures will be analysed by the IP method.

ACKNOWLEDGEMENTS

The authors would like to thank Professor H. Miyaji and Mr M. Inamori of Kyoto University for providing the PE single crystals. This work was financially supported by a grant for special equipment from the Ministry of Education, Science and Culture, Japan.

REFERENCES

1 Reimer, L. 'Transmission Electron Microscopy', 2nd Edn, Springer, Berlin, 1989, p. 450
2 Fujiyoshi, Y., Kobayashi, T., Uyeda, N., Ishida, Y. and Harada, Y. *Ultramicroscopy* 1980, **5**, 459
3 Sonoda, M., Takano, T., Miyahara, J. and Kato, H. *Radiology* 1983, **148**, 833

4 Amemiya, Y., Wakabayashi, K., Tanaka, H., Ueno, Y. and Miyahara, J. *Science* 1987, **237**, 164
5 Amemiya, Y. and Miyahara, J. *Nature* 1988, **336**, 89
6 Ichihara, S., Hayakawa, S., Saga, S., Hoshino, M., Sakuma, S., Ikeda, M., Yamaguchi, H., Hanaichi, T. and Kamiya, Y. *J. Electron Microsc.* 1984, **33**, 255
7 Hayakawa, S., Ichirara, S., Hoshino, M., Yamaguchi, H., Sakuma, S., Hanaichi, T., Kamiya, Y. and Arii, T. *J. Electron Microsc.* 1987, **36**, 1
8 Mori, N., Oikawa, T., Katoh, T., Miyahara, J. and Harada, Y. *Ultramicroscopy* 1988, **25**, 195
9 Isoda, S., Saitoh, K., Moriguchi, S. and Kobayashi, T. *Ultramicroscopy* 1991, **35**, 329
10 Isoda, S., Saitoh, K., Ogawa, T., Moriguchi, S. and Kobayashi, T. *Ultramicroscopy* 1992, **41**, 99
11 Hauptman, H. A. 'Crystal Structure Determination, The Role of the Cosine Seminvariants', Plenum Press, New York, 1972
12 Dorset, D. L. and Hauptman, H. A. *Ultramicroscopy* 1976, **1**, 195
13 Dorset, D. L. *Macromolecules* 1992, **25**, 4425
14 Dorset, D. L., Tivol, W. F. and Turner, J. N. *Acta Crystallogr.* 1992, **A48**, 562
15 Kavesh, S. and Schultz, J. M. *J. Polym. Sci. A2* 1970, **8**, 243
16 Kawaguchi, A., Ohara, M. and Kobayashi, K. *J. Macromol. Sci. B* 1979, **16**, 193
17 Phillips, P. J. and Tseng, H. T. *Polymer* 1985, **26**, 650